



# Photothermal Treatment of Polydopamine Nanoparticles@Hyaluronic Acid Methacryloyl Hydrogel Against Peripheral Nerve Adhesion in a Rat Model of Sciatic Nerve

Yongxin Zhan <sup>1,2</sup>, Zekun Zhou <sup>1,2</sup>, Miao Chen <sup>1,2</sup>, Xu Gong <sup>1,2</sup>

<sup>1</sup>Department of Hand and Podiatric Surgery, Orthopedics Center, The First Hospital of Jilin University, Changchun, 130021, People's Republic of China; <sup>2</sup>Jilin Province Key Laboratory on Tissue Repair, Reconstruction and Regeneration, The First Hospital of Jilin University, Changchun, 130021, People's Republic of China

Correspondence: Xu Gong, Department of Hand and Podiatric Surgery, Orthopedics Center, The First Hospital of Jilin University, 1 Xin Min Street, Changchun, Jilin, 130021, People's Republic of China, Tel +86 13944099151, Email gongxu@jlu.edu.cn

**Purpose:** Peripheral nerve adhesion occurs following injury and surgery. Functional impairment leading by peripheral nerve adhesion remains challenging for surgeons. Local tissue overexpression of heat shock protein (HSP) 72 can reduce the occurrence of adhesion. This study aims to develop a photothermal material polydopamine nanoparticles@Hyaluronic acid methacryloyl hydrogel (PDA NPs@HAMA) and evaluate their efficacy for preventing peripheral nerve adhesion in a rat sciatic nerve adhesion model.

**Materials and Methods:** PDA NPs@HAMA was prepared and characterized. The safety of PDA NPs@HAMA was evaluated. Seventy-two rats were randomly assigned to one of the following four groups: the control group; the hyaluronic acid (HA) group; the polydopamine nanoparticles (PDA) group and the PDA NPs@HAMA group (n = 18 per group). Six weeks after surgery, the scar formation was evaluated by adhesion scores and biomechanical and histological examinations. Nerve function was assessed with electrophysiological examination, sensorimotor analysis and gastrocnemius muscle weight measurements.

**Results:** There were significant differences in the score on nerve adhesion between the groups ( $p < 0.001$ ). Multiple comparisons indicated that the score was significantly lower in the PDA NPs@HAMA group (95% CI: 0.83, 1.42) compared with the control group (95% CI: 1.86, 2.64;  $p = 0.001$ ). Motor nerve conduction velocity and muscle compound potential of the PDA NPs@HAMA group were higher than the control group's. According to immunohistochemical analysis, the PDA NPs@HAMA group expressed more HSP72, less  $\alpha$ -smooth muscle actin ( $\alpha$ -SMA), and had fewer inflammatory reactions than the control group.

**Conclusion:** In this study, a new type of photo-cured material with a photothermic effect was designed and synthesized-PDA NPs@HAMA. The photothermic effect of PDA NPs@HAMA protected the nerve from adhesion to preserve the nerve function in the rat sciatic nerve adhesion model. This effectively prevented adhesion-related damage.

**Keywords:** peripheral nerve adhesion, sciatic nerve, HSP72, PDA, PTT, HA

## Introduction

Peripheral nerve adhesion is a common complication following peripheral nerve injury and surgery,<sup>1</sup> which often leads to functional impairment and paresthesia.<sup>2</sup> Adhesion mainly results from the excessive aggregation of fibrous tissue around the nerve,<sup>3</sup> which can cause neurodegenerative changes at the distal end of the nerve adhesion.<sup>4-6</sup> Clinically, external neurolysis is the standard operation for an established nerve adhesion;<sup>7-9</sup> to protect it against recurring adhesion, a muscle flap, adipofascial flap, or an autogenous vein is needed to cover or wrap the injured nerve.<sup>10-13</sup> Despite this, recurring adhesion remains a challenging issue in the clinical setting.<sup>14</sup> Therefore, some researchers have developed biological materials to prevent peripheral nerve adhesion. For instance, human amniotic fluid<sup>15</sup> or amniotic membrane,<sup>16</sup> acellular matrix films,<sup>17</sup> electrospun polycaprolactone (PCL)-amion nanofibrous membranes,<sup>5</sup> absorbable nerve ducts,<sup>18</sup>

and hydrogel<sup>19</sup> are some materials being developed. However, these materials are still at the experimental research stage due to the drawbacks of immunogenicity, infection risk, limitation of nerve slip, difficulty in obtaining methods, and different anti-adhesion abilities and therapeutic effects due to different target organs.<sup>5,15–19</sup>

In the study, we propose a novel therapeutic strategy to prevent nerve adhesion, namely, overexpression of heat shock protein (HSP) 72 by a photothermal material stimulating the nerve and its surrounding tissue may attenuate peripheral nerve adhesion. Zhou et al have demonstrated in animal models of renal fibrosis that overexpressed HSP72 inhibits fibroblast proliferation and differentiation by blocking the signal transducer and activator of transcription (STAT3) signaling pathway.<sup>20</sup> We therefore hypothesized that overexpressed HSP72 may block the STAT3 pathway and in turn inhibit differentiation from fibroblasts into myofibroblasts and reduce collagen production to attenuate peripheral nerve adhesion.

In the study, a novel photothermal material, namely, polydopamine nanoparticles@Hyaluronic acid methacryloyl hydrogel (PDA NPs@HAMA), has been developed to induce overexpressing HSP72 in the zone of may produce peripheral nerve adhesions by repetitive mild heat shock<sup>21</sup> (41 °C); to confirm the hypothesis mentioned above, a well-accepted animal model<sup>3</sup> of sciatic nerve adhesion was used to examine the degree of nerve adhesion, compound muscle action potential and sciatic function index.

## Materials and Methods

### Preparation of PDA NPs@HAMA

Hyaluronic acid methacryloyl hydrogel (HAMA) was synthesized according to the previous report.<sup>22</sup> Briefly, 4 g sodium hyaluronate (HA; Shanghai Yuanye Bio-Technology Co., Ltd) was completely dissolved in 200 mL PBS under magnetic stirring. Then 17 mL methacrylic anhydride was added dropwise into the solution in an ice water bath, during which pH of the solution was adjusted to 8–9 by 1M NaOH. The esterification reaction lasted for 3 h under continuous stirring in the dark, followed by 12 h at room temperature. The resulting solution was precipitated in excess ethanol, redissolved in deionized water, and dialysis in 10 kDa dialysis tube for 5 days. Finally, the HAMA solids could be obtained by lyophilizing the liquid in the bag for 48 h.

Polydopamine nanoparticles (PDA NPs) were synthesized through a classic approach.<sup>23</sup> Typically, 2 mL aqueous ammonia solution (NH<sub>4</sub>OH) was mixed with 40 mL ethanol and 90 mL deionized water under mild stirring. Then, 0.5 g dopamine hydrochloride (DA; Aladdin) was dissolved in 10 mL deionized water and injected into the solution. The reaction lasted for 24 h at room temperature. During the reaction, the solution color changed to a pale yellow and gradually turned to dark brown. The resulting solution was purified by centrifugation at 8800 rpm for 10 min and washed with deionized water three times. Finally, the powder of PDA NPs was obtained by drying the centrifuge sample at the bottom in an oven at 60 °C.

Polydopamine nanoparticles loaded with hyaluronic acid methacryloyl hydrogel (PDA NPs@HAMA) were fabricated by simply dispersing 0.5 mg PDA NPs in 10 mL 20 wt% HAMA precursor solution, which also contained 5 wt% photoinitiators 2-hydroxy-2-methyl-1-[4-(2-hydroxyethoxy) phenyl]-1-acetone (2959; Aladdin). The mixture solution was injected into the desired position and then irradiated for photocuring with a hand-held ultraviolet lamp for 1–2 min. The solution gradually became sticky during the process and finally formed a non-flowing gel.

### Characterization of PDA NPs@HAMA

The modification of HA was determined by nuclear magnetic resonance spectroscopy (<sup>1</sup>H NMR) and Fourier-transformed infrared spectroscopy (FTIR) on the Nicolet Avatar 360FTIR spectrophotometer. The internal structure of HAMA and PDA NPs@HAMA were examined by scanning electron microscope (SEM) on Hitachi SU-8020. The morphology of PDA NPs was observed by a high-resolution transmission electron microscope (TEM) on JEOL JEM-2100 F. Additionally, the UV-vis absorption curve of the PDA NPs solution was performed on Shimadzu 3100 UV-vis spectrophotometer. The photothermal curve was manually recorded and drawn by a commercial probe thermometer and an 808 nm laser device.

## The Biocompatibility of PDA NPs@HAMA

Rat Schwann cells (RSC96; the Type Culture Collection of the Chinese Academy of Sciences, Shanghai, China) were cultured in Dulbecco's modified Eagle's high glucose medium (DMEM, HyClone, USA) supplemented with 10% fetal bovine serum (FBS; Clark, USA), 1% penicillin-streptomycin (HyClone, USA). To obtain material leachate, different concentration of PDA NPs@HAMA (50 µg/mL, 100 µg/mL, 200 µg/mL) were soaked in serum-free high glucose DMEM under sterile conditions at 37 °C. After soaking for 24 h, the leaching liquid was collected and it was filtered before used.<sup>24</sup> Biocompatibility of PDA NPs@HAMA was tested using the Cell Counting Kit-8 and Calcein/PI Cell Viability/Cytotoxicity Assay Kit (Beyotime, China) according to the manufacturer's instructions. Organ H&E staining and blood routine test were also used to test the safety of the material.

## Study Design

Seventy-two adult male Sprague-Dawley rats (180–200 g; Liaoning Changsheng, China) were randomly assigned to the control group (no treatment), the hyaluronic acid group (HA; 0.5 mL of 10 mg/mL HA), the polydopamine nanoparticles group (PDA NPs; 4 mg), and PDA NPs@HAMA group (0.5 mL of 50 µg/mL PDA NPs@HAMA) (n = 18 per group). The animals were treated humanely based on the guidelines in the Guide for the Care and Use of Laboratory Animals published by the National Institutes of Health (USA). The rats were housed in individual cages at room temperature (23–25 °C) using ad libitum food pellets and water. The experimental protocol was approved by the Institutional Review Board of the Jilin University First Hospital (Approval No. 20220769).

## Animal Model

Rat sciatic nerve adhesion model was established according to the report of Shintani et al.<sup>3</sup> After eight hours of fasting, the rats were anesthetized with 2.5% isoflurane. The rats were placed in the left decubitus position. Under surgical loupe (1.5×), a 3 cm longitudinal skin incision was performed at the right thigh starting from the ischial tuberosity using a sterile technique. The right sciatic nerve was exposed by the intermuscular space between the superficial gluteus and the biceps femoris. After the sciatic nerve was dissected from the surface of the biceps femoris and protected by a 1×1 cm rubber sheet, the biceps femoris was burned repeatedly by a bipolar coagulator (Hög frekvens, China); the length of the biceps femoris burned was 1 cm. After cooling, the nerve was placed in situ and the intermuscular space was sutured by 6–0 absorbable suture (Jinhuan Medical, China). The skin incision was closed with 4–0 suture (Ethicon, China). All the left sciatic nerves underwent sham surgery, which involved nerves alone but without the adhesion procedure. After surgery, the rats mobilized freely in an individual cage without external immobilization. At the designated time, the rats were euthanized with an excessive anesthetic.

## Postoperative Photothermal Therapy (PPT)

From postoperative day 1, the rats in the PDA group and the PDA NPs@HAMA group were irradiated 20 minutes per day by NIR laser (808 nm, 0.48 W/cm<sup>2</sup>) for two weeks. The laser device was placed at 15 cm away from the site of nerve adhesion. The temperature of the nerve adhesion was maintained at 41.5 ± 0.5 °C,<sup>21,25,26</sup> which was monitored by FLIR T650sc camera (detector resolution: 640×480 pixels, wavelength range: 7.5–14 µm, FLIR Systems, Inc., Wilsonville, Ore.). This temperature can cause expression of heat shock proteins but it is not damage to skin. ([Supplement Figure 1](#))

## Evaluation of Nerve Adhesion at Six Weeks After Surgery

### Macroscopic Evaluation

Both wound healing and peripheral nerve adhesion were evaluated according to Petersen's scores.<sup>27</sup> The healing conditions of the skin incision was first examined and scored (1, skin or muscle fascia entirely closed; 2, skin or muscle fascia partially open; and 3, skin or muscle fascia completely open). Then the skin was incised along original incision to expose the sciatic nerve; the degree of nerve adhesion was scored (1, no adhesion or less adhesion; 2, some vigorous

blunt dissection required; and 3, sharp dissection required to separate the sciatic nerve from the surrounding tissue). The scores were performed by two blinded examiners and average scores were used in the analysis.

### Histological Evaluation

The rats were perfused through the heart with saline, followed by ice-cold 4% paraformaldehyde buffer. The sites of the nerve injury were harvested en bloc and immersed into 4% paraformaldehyde for 2 days, and then were embedded in paraffin. The specimens were sectioned transversely (3  $\mu$ m) and stained by hematoxylin and eosin (H&E) and Masson's trichrome, respectively. The area of collagen between the nerve and surrounding tissues was measured by ImageJ (200 $\times$ ).

### Biomechanical Evaluation

The adhesion strength between the nerve and surrounding tissue was evaluated by measuring the force detaching a fixed length of nerve from its bed.<sup>3</sup> The sciatic nerve was exposed through its original incision. After a nerve segment of 1 cm in length attaching its bed was left, the sciatic nerve was transected at its proximal and distal ends. The proximal nerve end was fixed to a digital dynamometer (WD-5; Wdgage, China) using 4-0 suture. The nerve segment was pulled until detaching from its bed, during which the peak force was recorded.

### Motor Function

Motor function was evaluated by means of the sciatic functional index (SFI),<sup>28</sup> which was measured based on footprints in walking track test. A SFI was calculated where 0 means normal motor function, less than 0 is a decrease in motor, and -100 is a total loss of motor function.

### Sensibility

The sensibility of both hindpaws of the rats was measured by means of Von Frey filament.<sup>29</sup> The rats were placed on a wire net platform in an individual cage. After the rats were habituated to the environment and were in a quite state, a Von Frey filament of 5 cm in length was used to stimulate the center of the hindpaw plantar skin to observe whether the withdrawal response occurred. If no response occurred for continuous three times, stopped and changed the filament in an order from the small to the large. The mechanical withdrawal threshold of both hindpaws, which was taken as the mean of three measurements, was the force (in grams) at which rats withdrew the paw in response to the stimulus. Then a withdrawal threshold index was calculated as the withdrawal threshold of the right hindpaw/ that of the left hindpaw (sham), where 100% means normal sensibility, and less than 100% is a decrease.

### Electrophysiology

The sciatic nerve was exposed along the original incision. The recording electrode was inserted into the gastrocnemius muscle. The electric stimulator (electrical pulses: 5 mA; duration: 0.1 ms; frequency: 1 Hz; Keypoint Neurological Instruments, Alpine bioMed Aps) was first placed proximal to the zone of nerve adhesion and then placed distal to the nerve adhesion, 10 mm distal to proximal stimulation. The compound muscle action potential and latency were recorded and the conduction velocity was calculated based on the difference of latency.

### Myelinated Axon Counts

The nerve specimens were harvested from the adhesion zones and fixed in 3% glutaraldehyde for 2 days. Then they were fixed in 1% osmium tetroxide for 2 h. After washing and dehydration, the specimens were embedded in epoxy resin media. The specimens were sectioned transversely (1  $\mu$ m) and stained with 1% toluidine blue. Under light microscope (BX51, Olympus, Japan), five high-power fields (1000 $\times$ ) were randomly captured by CellSens Dimension software (Olympus, Japan) and the total number of the myelinated axons was counted at each image by ImageJ software (NIH, Bethesda, MD, USA).

## Gastrocnemius at Six Weeks After Surgery

The gastrocnemius muscles on both sides were harvested and weighed. After fixation, dehydration and embedded in paraffin, the specimens were sectioned transversely (3  $\mu\text{m}$  in thickness) and stained with Masson's trichrome staining. Under light microscope (BX51, Olympus, Japan), six fields in each section were randomly chosen. The area of muscle fibers was measured using the ImageJ software (NIH, Bethesda, MD, USA).

## Immunohistochemistry Analysis

Immunohistochemistry was performed to assess the expression of HSP72, CD68 (activated macrophages marker), CD163 (marker for M2 macrophages), tumor necrosis factor  $\alpha$  (TNF- $\alpha$ ) and interleukin 1 $\beta$  (IL-1 $\beta$ ) (n = 3 per group) at two weeks after surgery and the expression of HSP 72 and  $\alpha$ -SMA (marker for myofibroblasts) at six weeks after surgery.

The sciatic nerves were harvested from the zone of adhesion. After formalin-fixed and paraffin-embedded, the specimens were cut longitudinally into tissue sections (3  $\mu\text{m}$  in thickness). After quenching of endogenous enzymes and antigen retrieval, the tissue sections were incubated with the antibodies against HSP72 (1:100; Enzo life Sciences), CD68 (1:100, Servicebio, China), CD163 (1:100, Servicebio, China), TNF- $\alpha$  (1:100, Servicebio, China), IL-1 $\beta$  (1:100, Servicebio, China), and  $\alpha$ -SMA (1: 400; Cell Signaling Technology) at 4  $^{\circ}\text{C}$  overnight. Then horseradish peroxidase-conjugated goat anti-rabbit antibodies were utilized as secondary antibodies. 3, 3-diaminobenzidine tetrahydrochloride (DAB; Zhongshan Golden Bridge Biotechnology, China) peroxidase substrate solution was used to visualize staining. The images were observed and photographed under a microscope, and high-power fields (200 $\times$ ) were chosen and captured. Quantitative analysis is the average optical density analysis after dyeing by ImageJ software.

## Statistical Analysis

Data were analyzed with IBM SPSS Statistics version 25 (IBM Corp., Armonk, NY, USA). The normality of residuals of the data was tested by the Shapiro–Wilk test. For data conformed to normal distribution, the data was expressed as mean  $\pm$  standard deviation (SD); comparisons between the groups were performed by one-way analysis of variance (ANOVA) or repeated-measures ANOVA, followed by Tukey's test. For data not conformed to normality, the data was expressed as median with range in parenthesis; the difference across the groups was compared using the Kruskal–Wallis test, followed by Mann–Whitney test with Bonferroni adjustment. A p-value < 0.05 was considered statistically significant.

## Results

### Characterization of PDA NPs@HAMA

Nuclear magnetic resonance spectroscopy ( $^1\text{H}$  NMR) results revealed that the emerging signals at 5.6 and 6.2 ppm in HAMA, belonging to the protons of  $-\text{CH}=\text{CH}_2$ , which confirmed that methacrylic acid was successfully connected to the skeleton of HA (Figure 1a).<sup>30</sup> Compared with HA, the stretching vibration band of C=O in HAMA was divided into two peaks, demonstrating the presence of anhydride (Figure 1b). The enhanced C-O-C stretching vibration also indicated that the ester bond was formed after modification, further verifying the conjugation of the carbon-carbon double bond in HAMA that endowed the cross-linkable and photocurable functions. It could be observed that the HAMA solution could be converted into a non-flowing gel under UV light irradiation for 1 min (Figure 1c). This ensured the stability and sustained release of PDA NPs when applying local nerve administration of PDA NPs@HAMA. The scanning electron microscopy (SEM) image of cured HAMA showed a porous scaffold structure, facilitating the exchange of nerve cells and tissue fluid. (Figure 1d) The synthesized PDA NPs appeared to have a uniformly dispersed nanospheres morphology with an average diameter of 160 nm under transmission electron microscopy (TEM) (Figure 1e).

The solution of PDA NPs was dark brown and possessed a broad absorption peak at 200–900 nm (Figure 1f). Therefore, it had a strong near-infrared photothermal conversion capacity. Under an 808 nm laser irradiation, the PDA NPs solution rapidly rose to 42  $^{\circ}\text{C}$  within 5 min (Figure 1g), which was a suitable temperature node for photothermal therapy without causing tissue damage.<sup>31</sup> Moreover, the HAMA solution doped with PDA NPs could also be photocured in 2 min under UV irradiation (Figure 1h). The longer gelling time was due to the darker solution color preventing the diffusion of light to some extent. In addition, the addition of PDA NPs did not affect the porous structure of the hydrogel

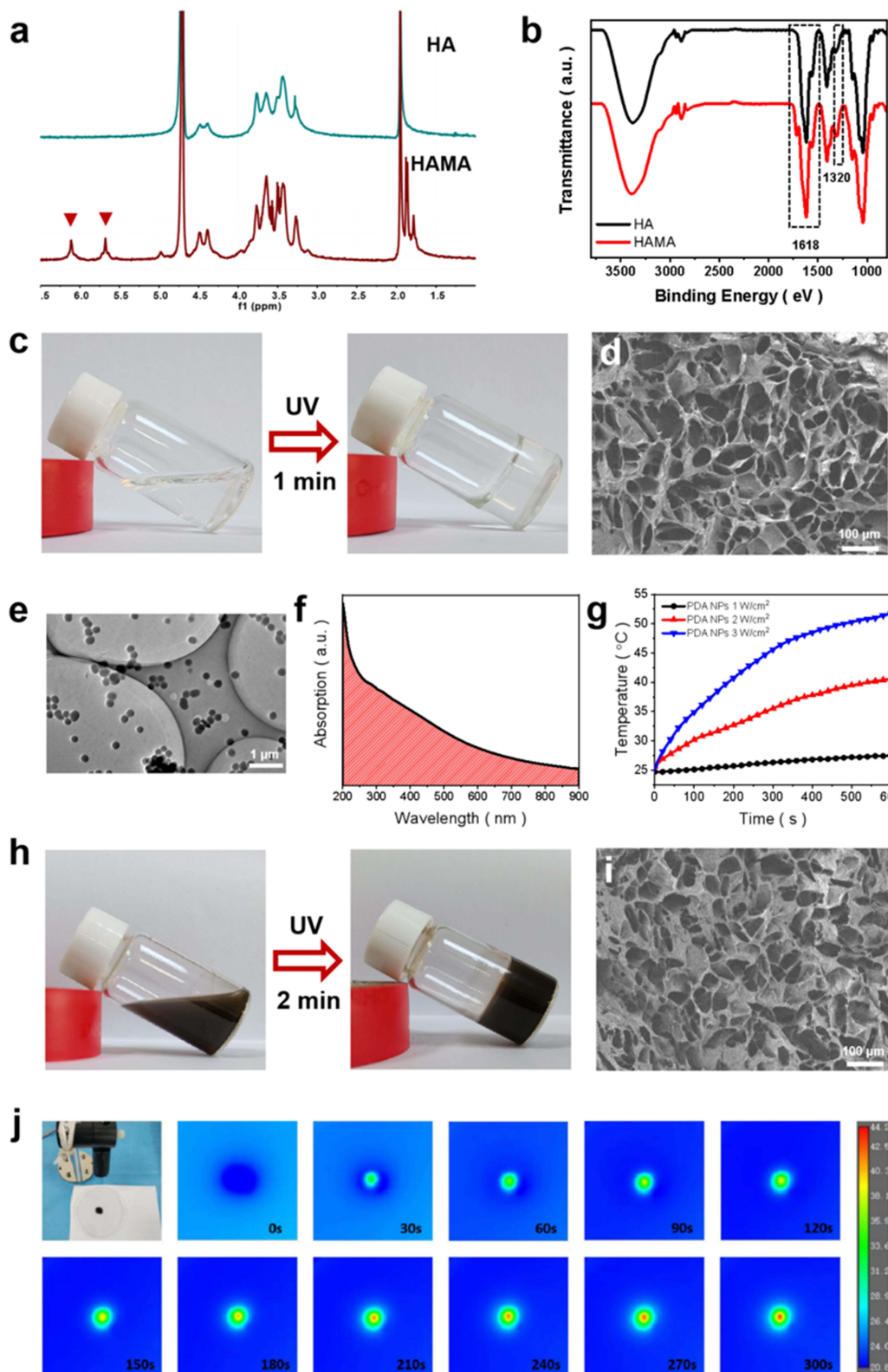


**Figure 1** Characterization of PDA NPs@HAMA. (a) The  $^1\text{H}$  NMR spectra of synthesized HA and HAMA. (b) The FT-IR spectrum of synthesized HA and HAMA. (c) The photograph of the HAMA solution before and after the hand-held UV lamp (365 nm) irradiation for 1 min. (d) The SEM image of HAMA after UV curing. (e) The TEM image of synthesized PDA NPs. (f) The UV-vis absorption spectra of PDA NPs. (g) The time-dependent temperature rise curve of PDA NPs solution (0.1 mg/mL) under 808 nm laser irradiation of different power. (h) The photograph of PDA NPs@HAMA solution before and after the hand-held UV lamp irradiation for 2 min. (i) The SEM image of PDA NPs@HAMA after UV curing. (j) The temperature-rising photographs of PDA NPs@HAMA gels taken by an infrared camera under 808 nm laser irradiation at low laser power density (0.48  $\text{W/cm}^2$ ).

(Figure 1i). As expected, the PDA NPs@HAMA gel exhibited good photothermal conversion ability. Furthermore, the temperature of PDA NPs@HAMA could quickly rise to 44 °C in 300 s of 808 nm laser irradiation with low power density. (Figure 1j) Based on the above results, a surgical dressing capable of in-situ curing and photothermal therapy has been successfully designed and fabricated.

## Biocompatibility of PDA NPs@HAMA

The results of the Calcein/PI Cell Viability/Cytotoxicity Assay Kit and Cell Counting Kit-8 are shown in Figure 2. Notably, cytoactive RSC96s were not influenced when RSC96 cells were co-cultured with extractions of PDA NPs@HAMA. Additionally, a great number of dead cells were not observed. As for cell viability, there was no statistical difference between the groups ( $p = 0.2258, 0.1901, 0.0723$ ). The results of organ H&E staining and blood routine are shown in Supplement Figure 2. The results showed no noticeable pathological changes in the rats after applying the material. Furthermore, there was no difference in blood routine results between the groups ( $p = 0.3339, 0.0881, 0.7384, 0.9429$ ).

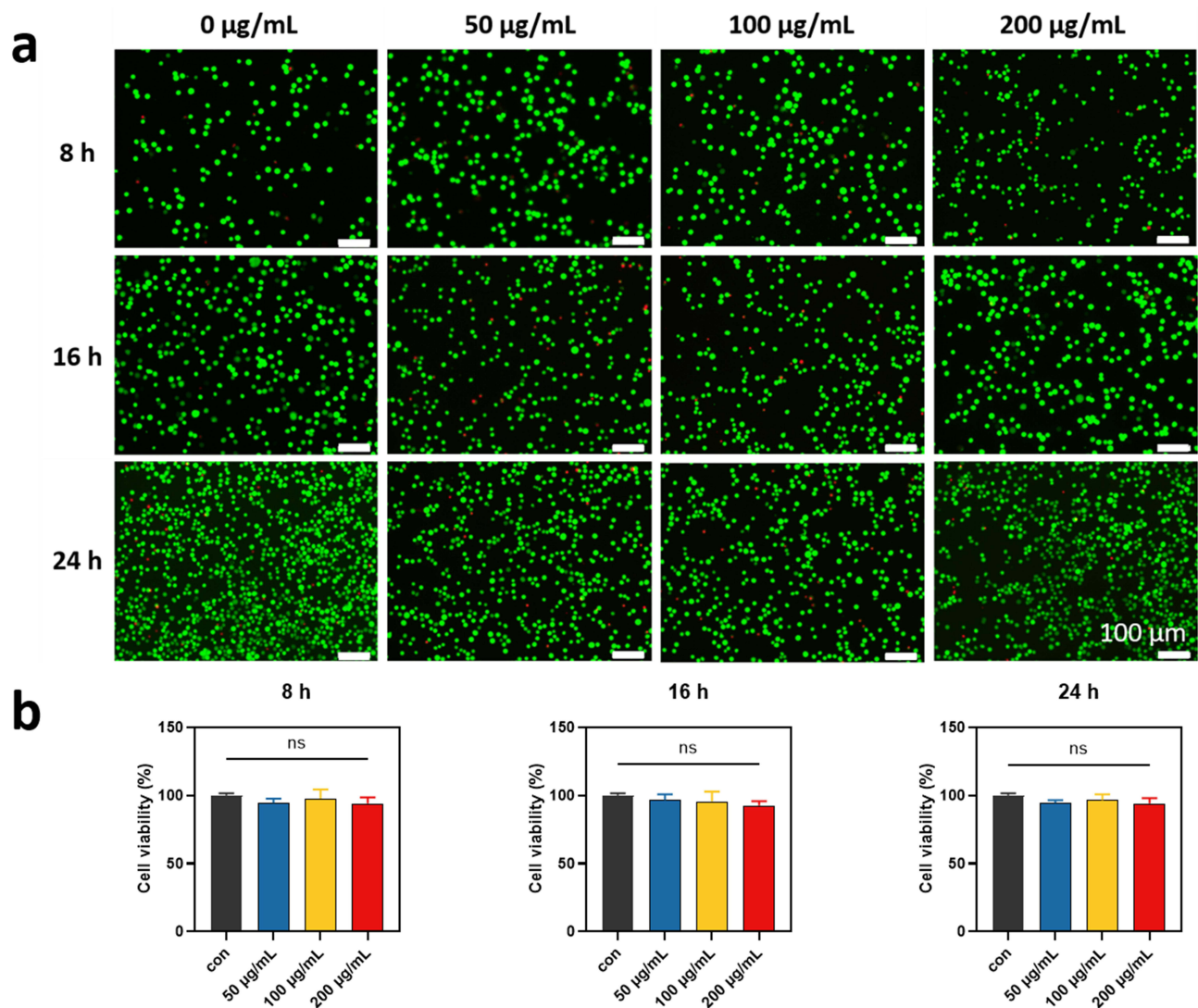


**Figure 2** Biocompatibility of PDA NPs@HAMA. (a) The Calcein/PI Cell Viability/Cytotoxicity Assay Kit results when RSC96 co-culture with extractions of PDA NPs@HAMA. (b) The results of Cell Counting Kit-8 when RSC96 co-culture with extractions of PDA NPs@HAMA.

**Abbreviation:** ns, no significance.

## Nerve Adhesion

### Macroscopic Evaluation

The time schedule of the peripheral nerve adhesion experiment is shown in Figure 3a. No infection or dehiscence was noted in all rats, but partial muscle dehiscence was observed in four rats ( $n = 3$  in the control group;  $n = 1$  in the PDA NPs@HAMA group). There was no significant difference in the scores on skin incisions among groups ( $p = 0.0842$ ,  $n = 6$  per group; Kruskal–Wallis test). Figure 3b illuminates gross appearances of the sciatic nerves at six weeks after surgery, and the statistical analysis results are shown in Figure 3d. In the control group there was a great deal of fibrous tissue covered the sciatic nerve. In the HA group, there was only a small amount of fibrous tissue. In the PDA group, there was no obvious fibrous tissue covering the nerve, but there was a significant PDA nanoparticle residual. In the PDA NPs@HAMA group, neither fibrous tissue nor PDA nanoparticles were noted. There was a significant difference in the score on nerve adhesion between the groups ( $p < 0.001$ ,  $n = 6$  per group; Kruskal–Wallis test). Multiple comparisons using Mann–Whitney test with Bonferroni adjust ( $0.05/6 = 0.0083$ ) indicated that the score was significantly greater in the control group compared with the HA group ( $p = 0.003$ ), the PDA group ( $p = 0.003$ ) and the PDA NPs@HAMA group ( $p = 0.001$ ), but there was no significant difference in the adhesion score among the HA group, the PDA group and the PDA NPs@HAMA group ( $p = 0.784$ ; Kruskal–Wallis test).

### Histological Evaluation

Figure 3c illuminates microscopic appearances between the nerve and surrounding tissue. Additionally, the statistical analysis results of Masson's trichrome are shown in Figure 3e. There was dense fibrous tissue between the nerve and surrounding tissue whereas there was loose fibrous tissue in the HA group, the PDA group and the PDA NPs@HAMA group. There was a significant difference in the area of collagen-positive between the groups ( $p < 0.001$ , one-way ANOVA,  $n = 3$  per group). The Tukey multiple comparisons showed that the mean area of collagen-positive between the nerve and surrounding tissue was the lowest in the sham group (mean  $\pm$  SD;  $14.66 \pm 2.20\%$ ), followed by the PDA group

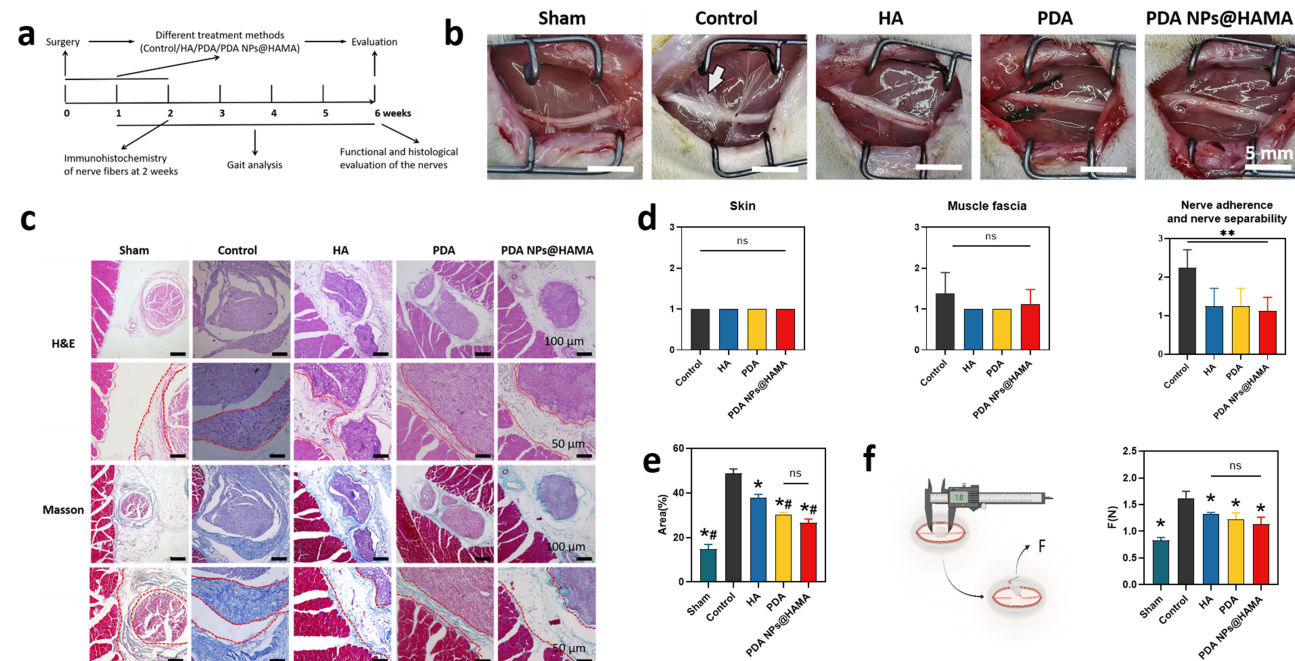


**Figure 3** Adhered analysis of peripheral nerve. (a) The time schedule of this study. (b) Typical illustration of gross adhesion score 6 weeks after surgery. The arrow shows the area with a large amount of scar tissue covering the sciatic nerve in the control group. (Scale bar: 5 mm) (c) The adhered nerve with surrounding tissue stained with hematoxylin and eosin (H&E) and Masson's trichrome. Representative micrographs are shown. The red dotted line shows the aggregation of fibrous tissue. (Scale bar: 100  $\mu$ m, 50  $\mu$ m) (d) Statistical analysis of the gross score of nerve adhesion. (\*\*vs control group,  $p < 0.01$ ). (e) Statistical analysis of the area of collagen after Masson's trichrome. (\*vs control group,  $p < 0.05$ , #vs HA group,  $p < 0.05$ ). (f) Biomechanical examination of the adhered nerve. Schematic diagram and statistical analysis results. (\*vs control group,  $p < 0.05$ ).

**Abbreviation:** ns, no significance.



( $30.11 \pm 1.17\%$ ) and the PDA NPs@HAMA group ( $26.54 \pm 1.71\%$ ), then the HA group ( $37.94 \pm 1.47\%$ ), and finally the control group ( $48.84 \pm 1.99\%$ ). There was no significant difference between the PDA group and the PDA NPs@HAMA group ( $p = 0.165$ ).

### Biomechanical Evaluation

Figure 3f illuminates the results of biomechanical test on nerve adhesion. As for the force of detaching the nerve from its bed, there was a significant difference between the groups ( $p < 0.001$ , one-way ANOVA,  $n = 3$  per group). The Tukey's test showed that the force of detaching the nerve from its bed was the lowest in the sham group ( $0.83 \pm 0.05$  N), followed by the HA group ( $1.32 \pm 0.03$  N), the PDA group ( $1.22 \pm 0.12$  N) and the PDA NPs@HAMA group ( $1.14 \pm 0.13$  N), and finally the control group ( $1.62 \pm 0.13$  N). There was no significant difference between the HA group, the PDA group and the PDA NPs@HAMA group ( $p = 0.26$ ).

### Motor Function

Figure 4a illuminates rats' tracks measured by a footprint test. There was a significant difference in SFI between different time points (repeated-measures ANOVA,  $p < 0.001$ ,  $n = 15$  per group). For the interaction between time and group, multivariate tests indicated that the interaction was statistically significant ( $p < 0.001$ ), suggesting that the SFI measured across the six different times was dependent on the groups. Figure 4b illustrates that the SFI showed a trend of continuous deterioration in the control group whereas in the other groups, the SFI showed a gradual improvement trend over time. In addition, there was a significant difference in the SFI across the four groups ( $p < 0.001$ ,  $n = 15$  per group); post hoc Tukey's test showed that the SFI was the highest in the PDA NPs@HAMA group, followed by the PDA group, then the HA group, and the lowest the control group.

### Sensibility

There was a significant difference in the withdrawal threshold index between different time points (repeated-measures ANOVA,  $p < 0.001$ ; Mauchly's test for sphericity:  $W = 0.764$ ,  $p = 0.408$ ;  $n = 15$  per group). The interaction between time and group was statistically significant ( $p = 0.042$ ), suggesting that the withdrawal threshold index across the six different times was dependent on the groups. Figure 4c illustrates that the withdrawal threshold of the right hindpaw was less than 60% of that of the left hindpaw (sham) in the control group whereas in the other groups it was more than 60%. In addition, there was a significant difference in the withdrawal threshold index across the four groups ( $p < 0.001$ ,  $n = 15$  per group); post hoc Tukey's test showed that the withdrawal threshold index in the control group was significantly lower than that in the HA group, the PDA group and the PDA NPs@HAMA group ( $p < 0.001$ ;  $p < 0.001$ ;  $p < 0.001$ ), but there was no significant difference between the HA group and the PDA NPs@HAMA group ( $p = 0.310$ ) and between the PDA group and the PDA NPs@HAMA group ( $p = 0.075$ ).

### Electrophysiology

The amplitude of the compound muscle action potential of the gastrocnemius muscles and the motor nerve conduction velocity are shown in Figure 5.

#### The Amplitude of CMAP

The amplitudes of CMAP were found to be different across groups (one-way ANOVA;  $p < 0.001$ ,  $n = 12$  per group). The Tukey multiple comparisons found that the mean amplitude was the greatest in the sham group ( $45.11 \pm 1.51$ ), followed by the PDA NPs@HAMA group ( $39.03 \pm 1.16$ ), then the PDA group ( $35.31 \pm 1.76$ ), then the HA group ( $27.92 \pm 2.29$ ), finally the control ( $21.46 \pm 2.33$ ).

#### The Velocity of Nerve Conduction

There was a significant difference in the velocity of nerve conduction across groups (Kruskal–Wallis test,  $p < 0.001$ ,  $n = 12$  per group). Multiple comparisons using Mann–Whitney test with Bonferroni adjust ( $0.05/12 = 0.004$ ) indicated that there was no significant difference in the velocity between the sham group and the PDA NPs@HAMA group ( $p = 0.006$ ) and between the PDA and the PDA NPs@HAMA group ( $p = 0.024$ ).

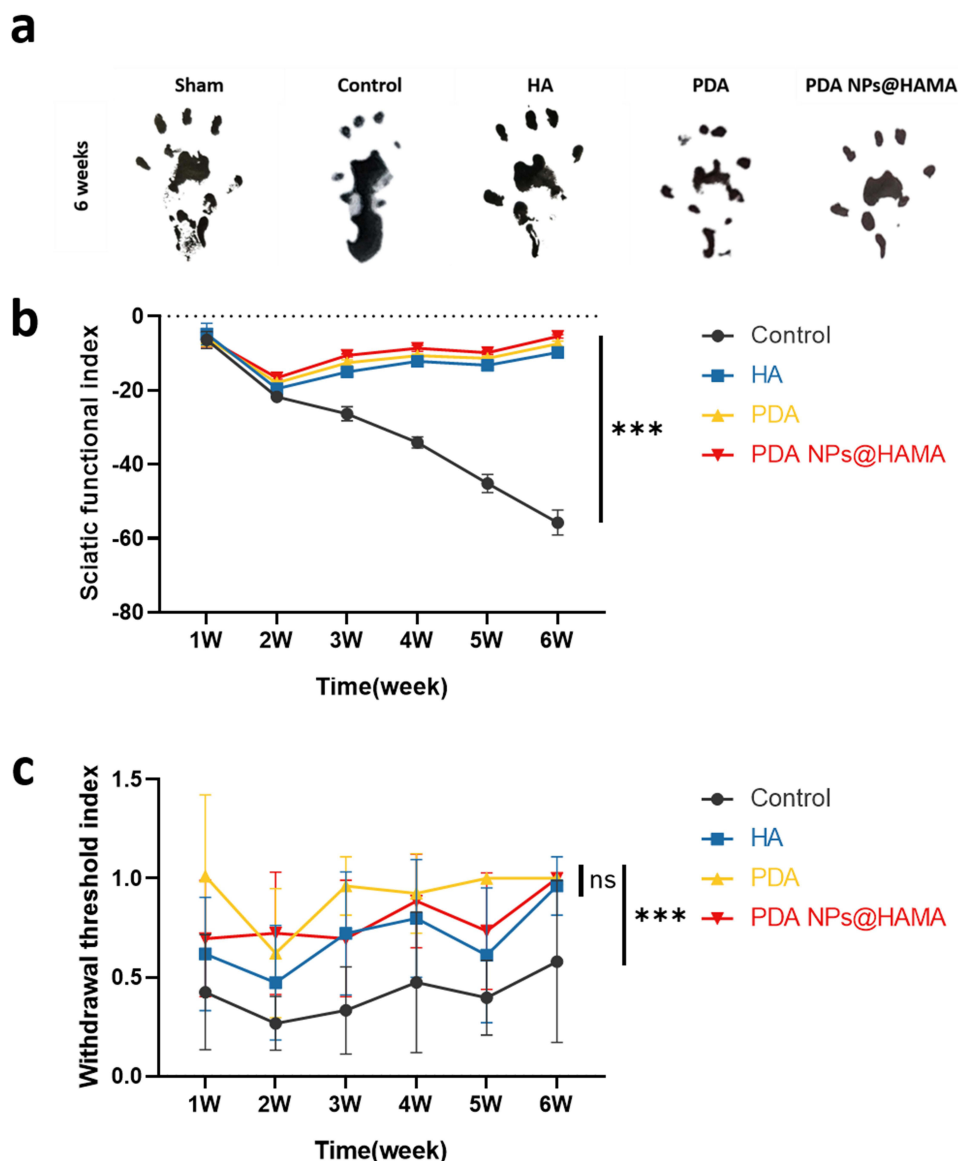


**Figure 4** Functional analysis of peripheral nerves. (a) Typical footprints of each group for footprint analysis at 6 weeks after surgery. (b) Statistical analysis of SFI. (\*\*\*)vs four groups,  $p < 0.001$ ) (c) Statistical analysis of withdrawal threshold index. (\*\*\*)vs four groups,  $p < 0.001$ ).

**Abbreviation:** ns, no significance.

## Myelinated Axon Counts

Axons in the adhesion nerve stained by 1% toluidine blue are shown in Figure 6a. The count of axons with myelin is shown in Figure 6b. There was a significant difference in myelinated axon counts across the groups (one-way ANOVA,  $p < 0.001$ ,  $n = 3$  per group). The Tukey multiple comparisons found that the counts was the greatest in the sham group ( $348.07 \pm 2.14$ ), followed by the PDA NPs@HAMA group ( $323.00 \pm 5.83$ ) and the PDA group ( $323.13 \pm 0.31$ ), then the HA group ( $243.80 \pm 8.66$ ), finally the control ( $158.00 \pm 1.00$ ).

## Relative Wet Weight of Gastrocnemius Muscles

Gastrocnemius muscles' representative images of gross appearance are shown in Figures 6c. Statistical analysis of the relative wet weight of gastrocnemius muscles is shown in Figure 6d. There was a significant difference in relative weight of gastrocnemius muscle across the groups (one-way ANOVA,  $p < 0.001$ ,  $n = 12$  per group). The Tukey multiple comparisons found that the counts was the greatest in the PDA NPs@HAMA group ( $95.65 \pm 0.02\%$ ), followed by the PDA group ( $92.17 \pm 0.01\%$ ), then the HA group ( $86.22 \pm 0.01$ ), finally the control ( $78.45 \pm 0.05$ ).

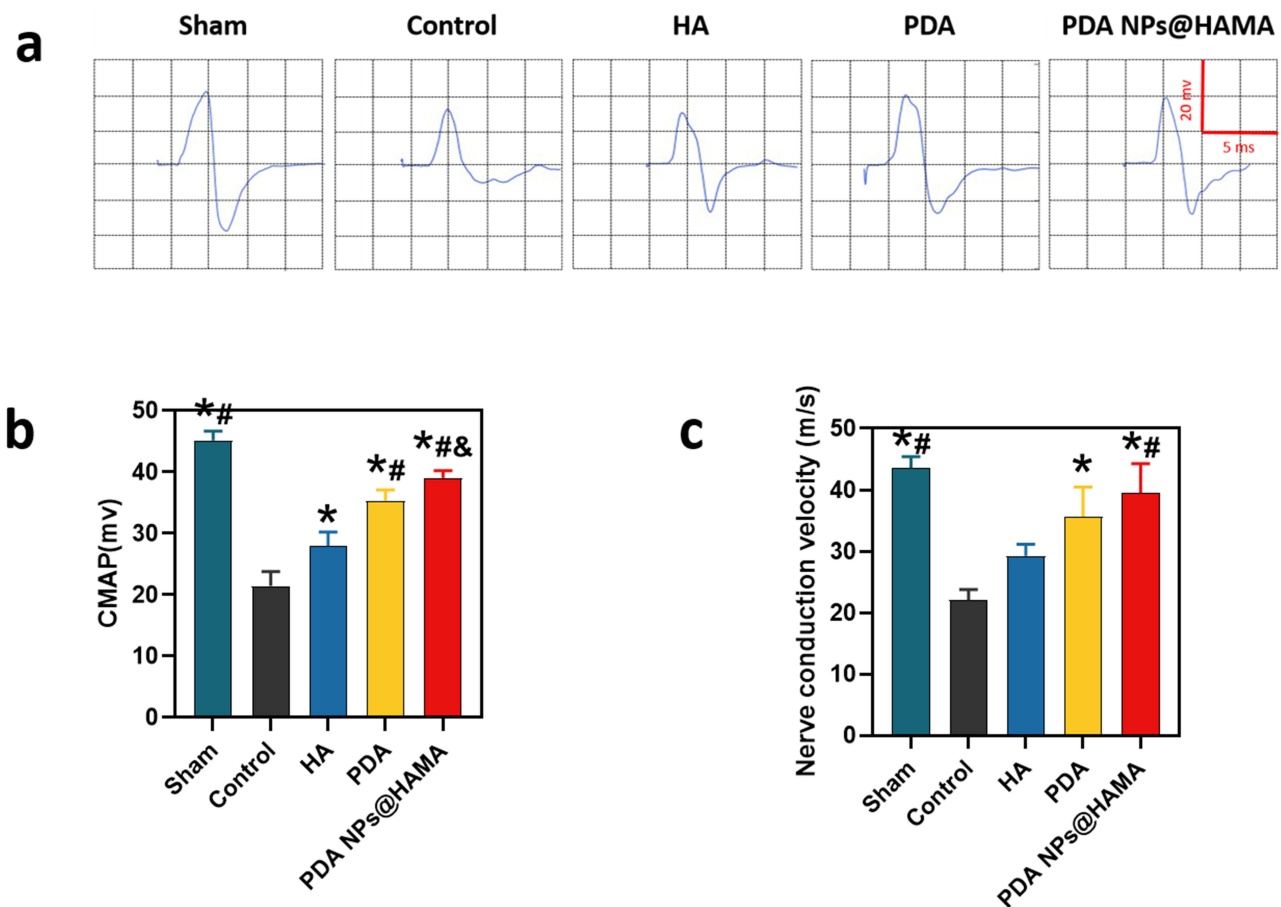


**Figure 5** Electrophysiology of sciatic nerves. (a) Typical waveforms of each group's Electrophysiological examination. (Scale bar: 20 mV, 5 ms) (b and c) Statistical analysis of electrophysiological examination. (\*vs control group, #vs HA group, &vs PDA group,  $p < 0.05$ ).

## Muscle Fiber Area Percentage of Gastrocnemius Muscles

Gastrocnemius muscles' representative images of histological appearance are shown in Figures 6e. The muscle fiber area percentage is shown in Figure 6f. There was a significant difference in muscle fiber area percentage of gastrocnemius muscle across the groups (one-way ANOVA,  $p < 0.001$ ,  $n = 3$  per group). The Tukey multiple comparisons found that the counts was the greatest in the sham group ( $75.13 \pm 1.07$ ), followed by PDA NPs@HAMA group ( $72.02 \pm 0.88$ ), then the PDA group ( $68.07 \pm 0.30$ ), then the HA group ( $59.85 \pm 0.78$ ), and finally the control ( $57.39 \pm 0.97$ ).

## Immunohistochemistry Analysis of Adhered Nerve

Typical pictures of immunohistochemistry of adhesion nerve tissue stained with the anti-HSP72 antibody at 2 weeks are shown in Figure 7a. Statistical analysis results are shown in Figure 7c. Typical pictures of immunohistochemistry of anti-HSP72 antibody and anti- $\alpha$ -SMA in Figure 7b. Statistical analysis results are shown in Figure 7d and e.

At 2 weeks after surgery (the end point of treatment), there was a significant difference in the average optical density of HSP72 across the groups (one-way ANOVA,  $p < 0.001$ ,  $n = 3$  per group). The Tukey multiple comparisons found that the average optical density was the greatest in the PDA NPs@HAMA group ( $0.26 \pm 0.01$ ), followed by the PDA group ( $0.21 \pm 0.00$ ), then the control group ( $0.19 \pm 0.01$ ), then the HA group ( $0.16 \pm 0.00$ ), and finally the sham group ( $0.11 \pm 0.00$ ).

At 6 weeks after surgery (the end point of the study), there was a significant difference in the average optical density of HSP72 and  $\alpha$ -SMA across the groups (one-way ANOVA,  $p < 0.001$ ,  $p < 0.001$ ,  $n = 3$  per group). The PDA NPs@HAMA group had more HSP72 ( $0.33 \pm 0.01$ ) expressed and less  $\alpha$ -SMA expressed ( $0.23 \pm 0.00$ ).

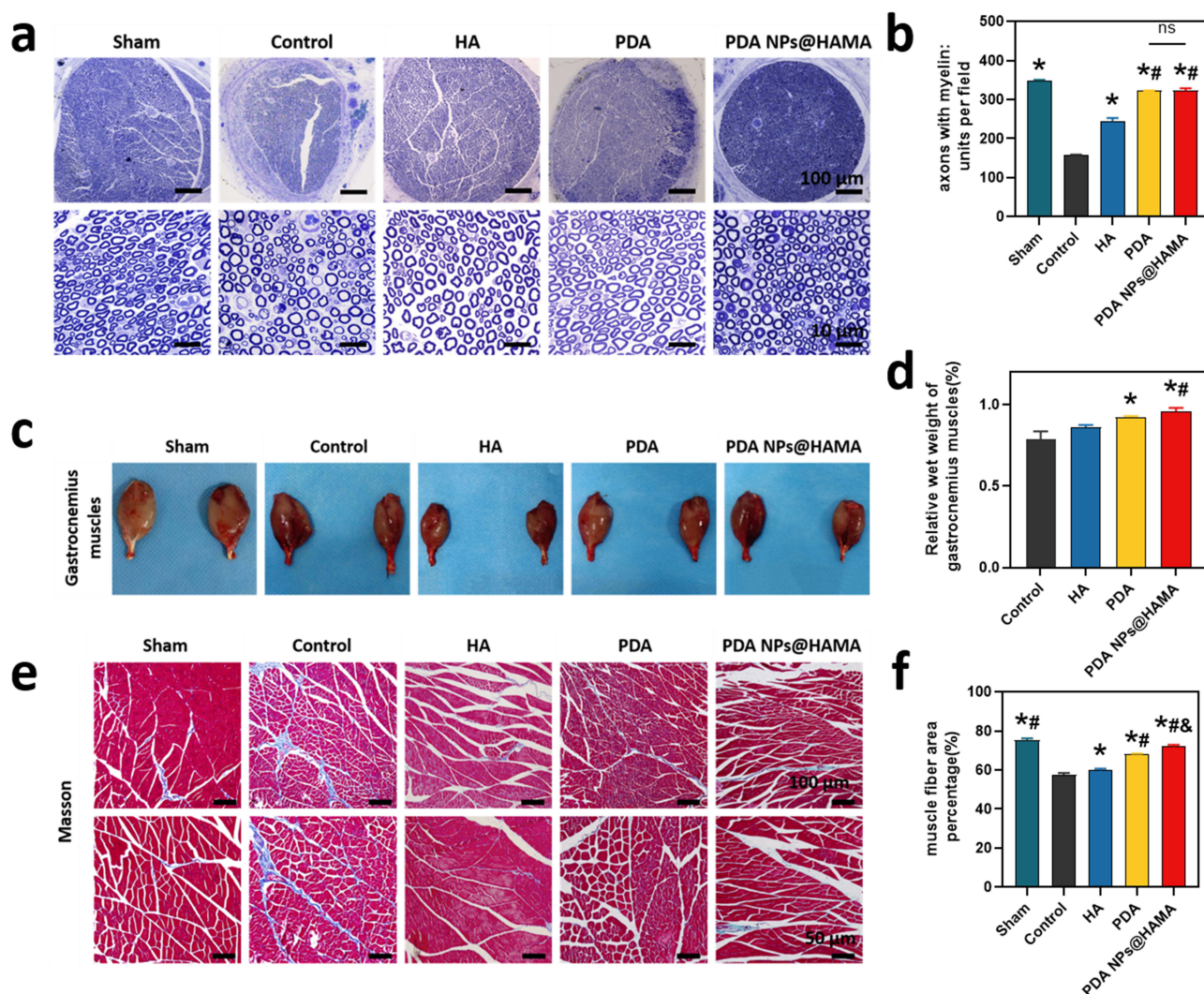


**Figure 6** Myelinated axon counts and analysis of gastrocnemius muscle. (a) Representative photomicrographs of axons stained using 1% toluidine blue at 6 weeks postoperatively. (Scale bar: 100  $\mu$ m, 10  $\mu$ m) (b) The count of axons with myelin. PDA group and PDA NPs@HAMA group had more axons with myelin than the others. (\*vs control group, #vs HA group,  $p < 0.05$ ) (c) Gastrocnemius muscles' representative images of gross appearance. (d) Statistical analysis of the relative wet weight of gastrocnemius muscles. (\*vs control group, #vs HA group) (e) Microscope image of gastrocnemius muscle cross-section characteristics with Masson trichromatic staining 6 weeks after surgery. (Scale bar: 100  $\mu$ m, 50  $\mu$ m) (f) The muscle fiber area percentage. (\*vs control group, #vs HA group, &vs PDA group,  $p < 0.05$ ). **Abbreviation:** ns, no significance.

As for inflammation, the results of the immunohistochemical evaluation of CD68, CD163, IL-1 $\beta$ , and TNF- $\alpha$  are shown in Figure 8. There was a significant difference in the average optical density of CD68, CD163, IL-1 $\beta$ , and TNF- $\alpha$  across the groups (one-way ANOVA,  $p < 0.001$ ,  $n = 3$  per group). The highest number of CD68-positive activated macrophages ( $2.66 \pm 0.01$ ) and more IL-1 $\beta$  ( $0.33 \pm 0.01$ ) and TNF- $\alpha$  ( $0.36 \pm 0.01$ ) positive expressions were found in the adhesion tissue in the control group. Additionally, more CD163-positive M2 macrophages ( $0.38 \pm 0.00$ ) and reduced IL-1 $\beta$  ( $0.23 \pm 0.00$ ) and TNF- $\alpha$  ( $0.25 \pm 0.00$ ) were found in the PDA NPs@HAMA group. Notably, the Tukey multiple comparisons found that there were statistical differences between the PDA NPs@HAMA group and the PDA group on the expressions of CD68, CD163, IL-1 $\beta$ , and TNF- $\alpha$  ( $p = 0.0109$ ,  $p < 0.0001$ ,  $p < 0.0001$ ,  $p = 0.0006$ , respectively).

## Discussion

Peripheral nerve adhesion often occurs after peripheral nerve injury and surgery. Nerve adhesion can cause axonal degeneration and affect nerve function, including conduction loss, target muscle function loss and motor neuron atrophy.<sup>32</sup> The recurrence of adhesions after surgery is also a significant problem for surgeons. Importantly, peripheral

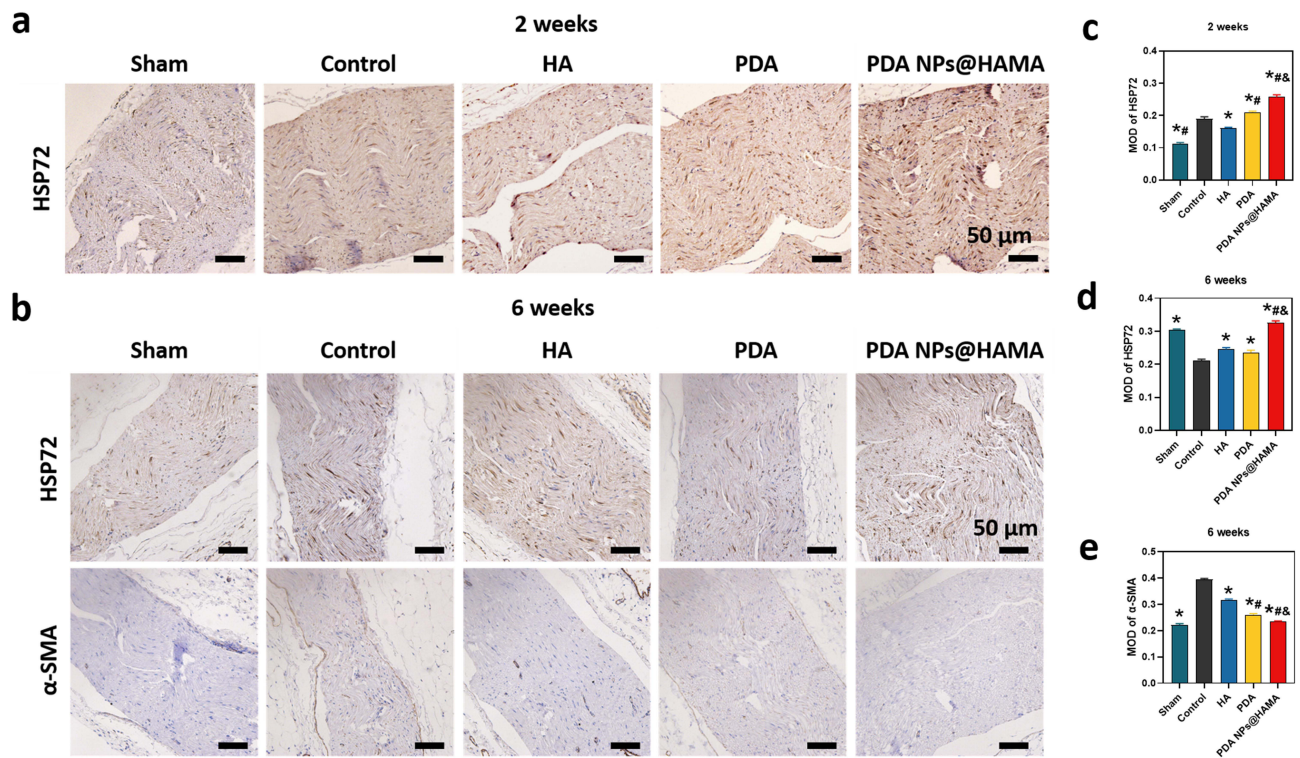


**Figure 7** Immunohistochemistry analysis of adhesion nerve. (a) Typical pictures of immunohistochemistry of adhesion nerve tissue stained with the anti-HSP72 antibody at 2 weeks. (Scale bar: 50 μm) (b) Typical pictures of immunohistochemistry of adhesion nerve tissue stained with the anti-HSP72 antibody and the anti-α-SMA antibody at 6 weeks postoperatively. (Scale bar: 50 μm) (c–e) Statistical analysis of anti-HSP72 antibody and anti-α-SMA antibody immunohistochemically evaluation. (\*vs control group, #vs HA group, &vs PDA group, p < 0.05).

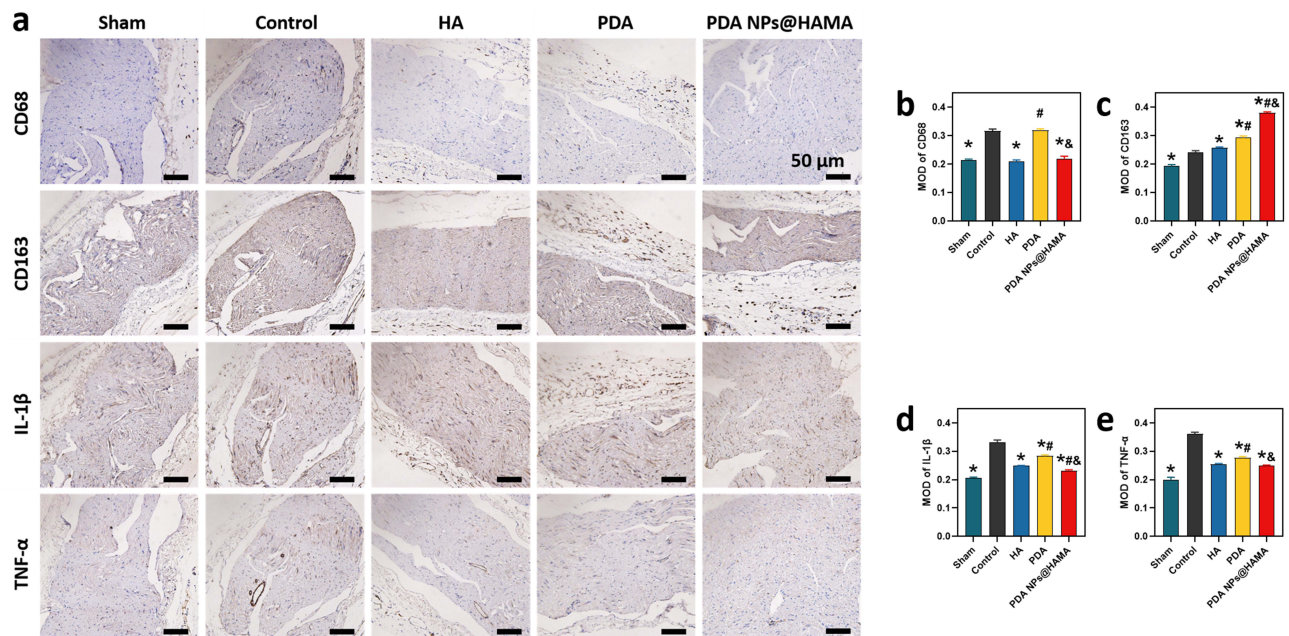


**Figure 8** Immunohistochemical evaluation of CD68, CD163, IL-1β, and TNF-α. (a) Typical pictures of immunohistochemistry of adhesion nerve tissue stained with anti-CD68 antibody, anti-CD163, anti-IL-1β, and anti-TNF-α at 2 weeks postoperatively. (Scale bar: 50 μm) (b–e) Statistical analysis results of the immunohistochemical evaluation of inflammatory markers. (\*vs control group, #vs HA group, &vs PDA group, p < 0.05).

nerve adhesion is caused by macrophage aggregation, fibroblast aggregation, and collagen production.<sup>3</sup> Therefore, it is worth reducing the inflammatory response and preventing the aggregation of fibers in the early stage of adhesion formation is worth considering.

At present, researchers have used vein encapsulation, fat encapsulation and other measures to reduce the occurrence of peripheral nerve adhesions such as buccal mucosa, which is a kind of biological materials.<sup>33</sup> There are also researchers using a variety of non-biological materials: silica gel, membrane, catheter, etc., to cover the nerve to prevent the growth of fibrous tissue around the nerve.<sup>34</sup> To date, these biomaterials have not yet been translated into clinic. Thus, photothermal therapy (PTT) is a new therapeutic strategy that uses stimulated photothermal materials to produce heat.<sup>35,36</sup> Notably, it is a convenient, non-invasive, and highly specific physiotherapy method with clinical applications.<sup>37</sup> The heating effect of photothermal therapy is more stable, and the temperature can be monitored and accurately controlled.<sup>38</sup> It is more in line with the postoperative treatment strategy, and it avoids the shortcomings of heating locally, uncontrollable internal temperature and large changes.<sup>39</sup> The production of heat by photothermal materials has a small heat impact area on the body and little thermal damage to the surrounding tissues, which has good biological safety.<sup>40</sup>

Heating can induce the increase of HSP72,<sup>41</sup> a member of the HSP70 family, is a stress-induced molecular chaperone capable of stabilizing and folding substrate proteins to maintain cellular homeostasis.<sup>42</sup> Heat stress can induce the upregulation of HSP72 in nucleated cells.<sup>43</sup> Importantly, HSP72 has been reported to be essential in inhibiting adhesion formation.<sup>20,43–45</sup> Previous studies have shown that heating treatment can induce an increase in HSP72 expression.<sup>46</sup>

The increased expression of HSP72 can increase the probability of survival of nerve-related cells.<sup>47</sup> PDA can be excited by an 808 nm near-infrared<sup>48</sup> laser to produce a photothermal effect, primarily used for tumor therapy. Studies have also shown that heating to 41–42 °C for 20 min can induce the production of heat shock proteins.<sup>21</sup> However, photothermal therapy has not been shown to reduce the production of peripheral nerve adhesions.

In this study, it was first confirmed that PDA NPs@HAMA had good biocompatibility without cytotoxicity. And then, further research showed that the modified material better inhibited the formation of adhesion tissue around the rat sciatic nerve, had a lower gross score, and better biomechanical performance. Additionally, the rats retained better neural function with fewer demyelinating changes and target muscle atrophy. In doing so, this therapy reduced the production of  $\alpha$ -SMA, inhibited the transformation of fibroblasts into myofibroblasts. Masson-stained tissue cross-sections yielded results consistent with the gross score, showing microscopic aggregation of fibers around the nerve.<sup>49</sup> Furthermore, immunohistochemical results of the adhesion nerve also indicated that photothermal therapy could reduce inflammation to a certain extent (Figure 9).

This study speculated that for the new material, hyaluronic acid gel inhibited the excessive induction of inflammation in the early stage and made PDA particles evenly distributed around nerves. The photothermal effect of PDA reduced collagen aggregation and ultimately reduced the adhesion of peripheral nerves.

PDA NPs@HAMA is a flexible, semi-solid adhesive that provides a physical barrier to peripheral nerves, thereby reducing peripheral nerve adhesion by preventing fibrous tissue growth. It is biocompatible and biodegradable, without rejection or inflammatory reaction, does not hinder the diffusion of nutrients, does not affect wound healing, avoids scar ischemia, promotes nerve slip, has no incidence of the donor area, is easy to obtain and prepare, stable in nature, strong in repeatability, and does not damage other parts of the body when applied locally. The new gel material developed in this study can not only be directly added during the operation, which can effectively reduce material leakage after light curing, but also can be used for local injection for conservative treatment and photothermal treatment under regular near-infrared excitation, which has a broad clinical application prospect. In addition, this material can be used as a drug sustained release system to load drugs, providing a basis for future research. When PDA was added to the hyaluronic acid gel, the material volume was increased, and the application of PDA was reduced so that there would be no prominent PDA clumps after the hyaluronic acid gel degradation 6 weeks after surgery (Supplement Figure 3). Therefore, applying hyaluronic acid can reduce the local inflammatory reaction of peripheral nerves to a certain extent.<sup>50</sup> Furthermore, its ability to suppress inflammation can help reduce the occurrence of adhesions.<sup>51</sup>

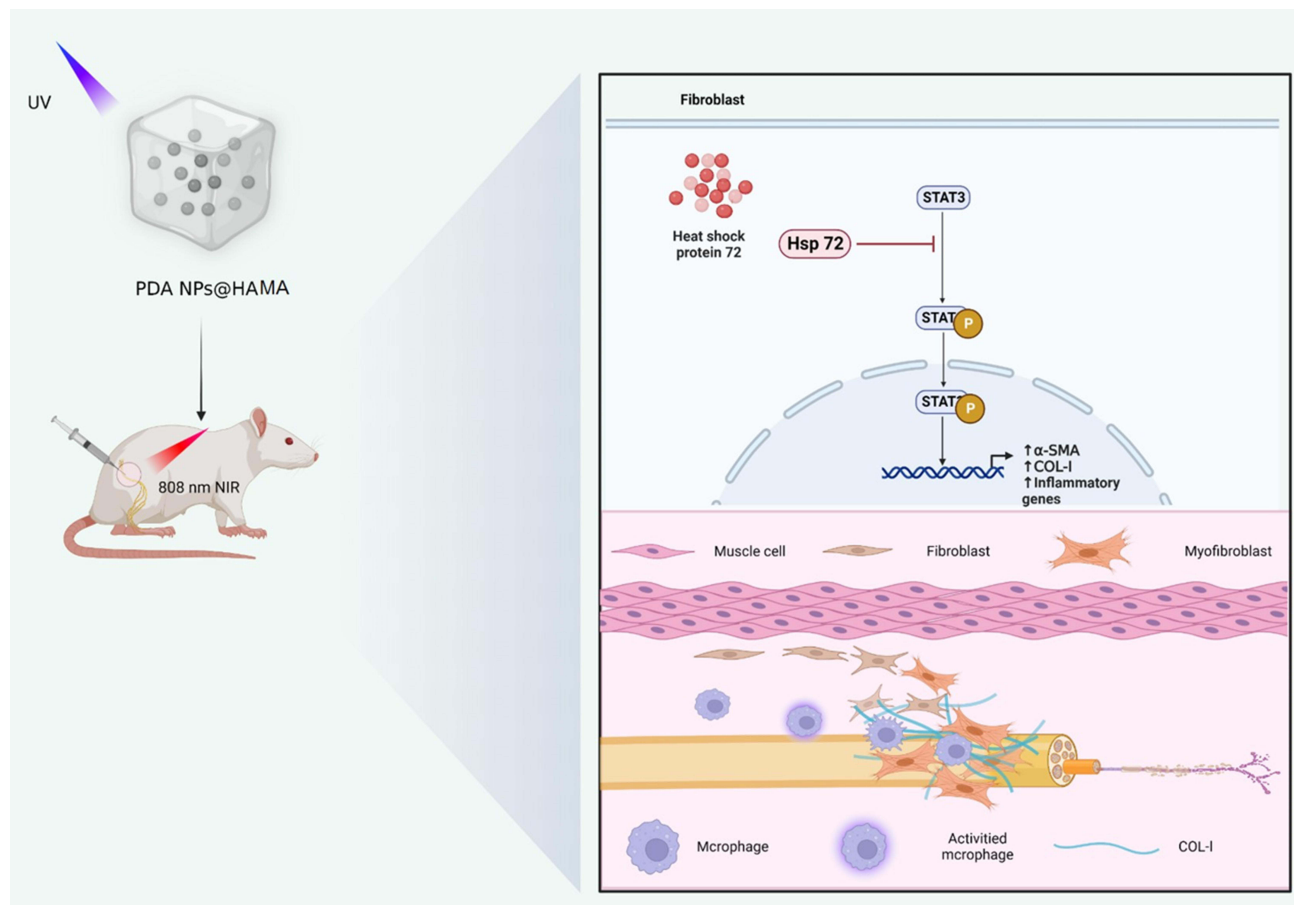


**Figure 9** Schematic of this study.

## Conclusion

This study designed and synthesized a new type of photo-cured material with a photothermic effect: PDA NPs@HAMA. The photothermic effect of PDA NPs@HAMA protected nerve adhesion and preserved the nerve function in the rat sciatic nerve adhesion model. Additionally, it effectively prevented adhesion-related damage. Notably, our research results provide a new therapeutic method for preventing peripheral nerve adhesion, which provides a theoretical basis and method support for the design and subsequent clinical application of the next generation of anti-adhesion or pro-regeneration materials.

## Acknowledgments

We would like to appreciate the technical help from the Central Laboratory and Department of Pathology, the First Hospital (Section 2) of Jilin University.

The preparation and characterization of PDA NPs@HAMA were performed by State Key Laboratory of Supramolecular Structure and Materials, College of Chemistry, Jilin University.

We would like to thank Dr. Mingxi Yang, Department of Hand and Podiatric Surgery, Orthopedics Center, First Hospital of Jilin University, for his important contribution in design, synthesis and characterization of PDA NPs@HAMA.

## Disclosure

The authors report no conflicts of interest in this work.

## References

1. Lemke A, Ferguson J, Gross K, et al. Transplantation of human amnion prevents recurring adhesions and ameliorates fibrosis in a rat model of sciatic nerve scarring. *Acta Biomater.* 2018;66:335–349. doi:10.1016/j.actbio.2017.11.042
2. Ohsumi H, Hirata H, Nagakura T, et al. Enhancement of perineurial repair and inhibition of nerve adhesion by viscous injectable pure alginate sol. *Plast Reconstr Surg.* 2005;116(3):823–830. doi:10.1097/01.prs.0000176893.44656.8e
3. Shintani K, Uemura T, Takamatsu K, et al. Protective effect of biodegradable nerve conduit against peripheral nerve adhesion after neurolysis. *J Neurosurg.* 2018;129(3):815–824. doi:10.3171/2017.4.JNS162522
4. Abe Y, Doi K, Kawai S. An experimental model of peripheral nerve adhesion in rabbits. *Br J Plast Surg.* 2005;58(4):533–540. doi:10.1016/j.bjps.2004.05.012
5. Dong R, Liu C, Tian S, et al. Electrospun polycaprolactone (PCL)-amnion nanofibrous membrane prevents adhesions and promotes nerve repair in a rat model of sciatic nerve compression. *PLoS One.* 2020;15(12):e0244301. doi:10.1371/journal.pone.0244301
6. Hellebrekers BW, Kooistra T. Pathogenesis of postoperative adhesion formation. *Br J Surg.* 2011;98(11):1503–1516. doi:10.1002/bjs.7657
7. Yan JG, Logiudice J, Davis J, et al. Calcitonin pump improves nerve regeneration after transection injury and repair. *Muscle Nerve.* 2015;51(2):229–234. doi:10.1002/mus.24281
8. Papatheodorou LK, Williams BG, Sotereanos DG. Preliminary results of recurrent cubital tunnel syndrome treated with neurolysis and porcine extracellular matrix nerve wrap. *J Hand Surg Am.* 2015;40(5):1264–1272. doi:10.1016/j.jhsa.2015.02.031
9. Kikuchi K, Setoyama K, Takada S, et al. E8002 inhibits peripheral nerve adhesion by enhancing fibrinolysis of l-ascorbic acid in a rat sciatic nerve model. *Int J Mol Sci.* 2020;21(11):3972. doi:10.3390/ijms21113972
10. Soltani AM, Allan BJ, Best MJ, Mir HS, Panthaki ZJ. A systematic review of the literature on the outcomes of treatment for recurrent and persistent carpal tunnel syndrome. *Plast Reconstr Surg.* 2013;132(1):114–121. doi:10.1097/PRS.0b013e318290fab
11. Xu J, Varitimidis SE, Fisher KJ, Tomaino MM, Sotereanos DG. The effect of wrapping scarred nerves with autogenous vein graft to treat recurrent chronic nerve compression. *J Hand Surg Am.* 2000;25(1):93–103. doi:10.1053/jhsu.2000.jhsu025a0093
12. Kokkalis ZT, Jain S, Sotereanos DG. Vein wrapping at cubital tunnel for ulnar nerve problems. *J Shoulder Elbow Surg.* 2010;19(2 Suppl):91–97. doi:10.1016/j.jse.2009.12.019
13. Dy CJ, Aunins B, Brogan DM. Barriers to epineurial scarring: role in treatment of traumatic nerve injury and chronic compressive neuropathy. *J Hand Surg Am.* 2018;43(4):360–367. doi:10.1016/j.jhsa.2018.01.013
14. Amadio PC. Interventions for recurrent/persistent carpal tunnel syndrome after carpal tunnel release. *J Hand Surg Am.* 2009;34(7):1320–1322. doi:10.1016/j.jhsa.2009.04.031
15. Ozgenel GY, Filiz G. Effects of human amniotic fluid on peripheral nerve scarring and regeneration in rats. *J Neurosurg.* 2003;98(2):371–377. doi:10.3171/jns.2003.98.2.0371
16. Gaspar MP, Abdelfattah HM, Welch IW, Vosbikian MM, Kane PM, Rekan MS. Recurrent cubital tunnel syndrome treated with revision neurolysis and amniotic membrane nerve wrapping. *J Shoulder Elbow Surg.* 2016;25(12):2057–2065. doi:10.1016/j.jse.2016.09.013
17. Shin YH, Yun HW, Park SY, et al. Effect of glutaraldehyde-crosslinked cartilage acellular matrix film on anti-adhesion and nerve regeneration in a rat sciatic nerve injury model. *J Tissue Eng Regen Med.* 2021;15(11):1023–1036. doi:10.1002/term.3249
18. Lee JY, Parisi TJ, Friedrich PF, Bishop AT, Shin AY. Does the addition of a nerve wrap to a motor nerve repair affect motor outcomes? *Microsurgery.* 2014;34(7):562–567. doi:10.1002/micr.22274
19. Urano H, Iwatsuki K, Yamamoto M, et al. Novel anti-adhesive CMC-PE hydrogel significantly enhanced morphological and physiological recovery after surgical decompression in an animal model of entrapment neuropathy. *PLoS One.* 2016;11(10):e0164572. doi:10.1371/journal.pone.0164572
20. Zhou Y, Cao S, Li H, et al. Heat shock protein 72 antagonizes STAT3 signaling to inhibit fibroblast accumulation in renal fibrogenesis. *Am J Pathol.* 2016;186(4):816–828. doi:10.1016/j.ajpath.2015.11.016
21. Healy C, Mulhall KJ, Fitz Patrick D, Kay EW, Bouchier-Hayes D. The effect of thermal preconditioning of the limb on flexor tendon healing. *J Hand Surg Eur Vol.* 2007;32(3):289–295. doi:10.1016/J.JHSB.2007.01.004
22. Liu X, Wei Y, Xuan C, et al. A biomimetic biphasic osteochondral scaffold with layer-specific release of stem cell differentiation inducers for the reconstruction of osteochondral defects. *Adv Healthc Mater.* 2020;9(23):e2000076. doi:10.1002/adhm.202000076
23. Liu Y, Ai K, Liu J, Deng M, He Y, Lu L. Dopamine-melanin colloidal nanospheres: an efficient near-infrared photothermal therapeutic agent for in vivo cancer therapy. *Adv Mater.* 2013;25(9):1353–1359. doi:10.1002/adma.201204683
24. Zhou C, Xu AT, Wang DD, Lin GF, Liu T, He FM. The effects of Sr-incorporated micro/nano rough titanium surface on rBMSC migration and osteogenic differentiation for rapid osteointegration. *Biomater Sci.* 2018;6(7):1946–1961. doi:10.1039/c8bm00473k
25. Tang XM, Dai J, Sun HL. Thermal pretreatment promotes the protective effect of HSP70 against tendon adhesion in tendon healing by increasing HSP70 expression. *Mol Med Rep.* 2019;20(1):205–215. doi:10.3892/mmr.2019.10240
26. McLaughlin R, Kay E, Kiely P, Bouchier-Hayes D, Murray P. Thermal preconditioning prevents peritendinous adhesions and inflammation. *Clin Orthop Relat Res.* 2002;405:258–266. doi:10.1097/01.blo.0000022175.66847.40
27. Petersen J, Russell L, Andrus K, MacKinnon M, Silver J, Kliot M. Reduction of extraneural scarring by ADCON-T/N after surgical intervention. *Neurosurgery.* 1996;1996(38):976–984. doi:10.1097/00006123-199605000-00025
28. Bain JR, Mackinnon SE, Hunter DA. Functional evaluation of complete sciatic, peroneal, and posterior tibial nerve lesions in the rat. *Plast Reconstr Surg.* 1988;83:129–136. doi:10.1097/00006534-198901000-00024
29. Cobianchi S, de Cruz J, Navarro X. Assessment of sensory thresholds and nociceptive fiber growth after sciatic nerve injury reveals the differential contribution of collateral reinnervation and nerve regeneration to neuropathic pain. *Exp Neurol.* 2014;255:1–11. doi:10.1016/j.expneurol.2014.02.008
30. Zeng AS, Johnson M, Johnson M, et al. Green synthetic approach for photo-cross-linkable methacryloyl hyaluronic acid with a tailored substitution degree. *Biomacromolecules.* 2020;21(6):2229–2235. doi:10.1021/acs.biomac.0c00196
31. Li L, Zhang X, Zhou J, Zhang L, Xue J, Tao W. Non-invasive thermal therapy for tissue engineering and regenerative medicine. *Small.* 2022;18(36). doi:10.1002/smll.202107705
32. Ghosh N, Bregere C, Bustos P, Guzman R. L-Ala-L-Gln Suppresses hypoxic phenotype and fibrogenic activity of rat perineurial fibroblasts. *CNS Neurol Disord Drug Targets.* 2022. doi:10.2174/1871527321666220414094149
33. Baltu Y, Uzun H, Ozgenel GY. The reduction of extraneural scarring with buccal mucosa graft wrapping around the sciatic nerve: an experimental study in a rat model. *J Plast Surg Hand Surg.* 2017;51(4):259–263. doi:10.1080/2000656X.2016.1241790



34. Dam-Hieu P, Lacroix C, Said G, Devanz P, Liu S, Tadie M. Reduction of postoperative perineural adhesions by Hyaloglide gel: an experimental study in the rat sciatic nerve. *Neurosurgery*. 2005;56(2Suppl):425–33;discussion 425–33. doi:10.1227/01.neu.0000156845.41626.e9
35. Lu J, Cai L, Dai Y, et al. Polydopamine-based nanoparticles for photothermal therapy/chemotherapy and their synergistic therapy with autophagy inhibitor to promote antitumor treatment. *Chem Rec*. 2021;21(4):781–796. doi:10.1002/tcr.202000170
36. Shakeri-Zadeh A, Kamrava SK, Farhadi M, Hajikarimi Z, Maleki S, Ahmadi A. A scientific paradigm for targeted nanophotothermolysis; the potential for nanosurgery of cancer. *Lasers Med Sci*. 2014;29(2):847–853. doi:10.1007/s10103-013-1399-x
37. Fang D, Li T, Wu Z, et al. Dual drive mode polydopamine nanomotors for continuous treatment of an inferior vena cava thrombus. *J Mater Chem B*. 2021;9(41):8659–8666. doi:10.1039/d1tb01202a
38. Huo J, Jia Q, Huang H, et al. Emerging photothermal-derived multimodal synergistic therapy in combating bacterial infections. *Chem Soc Rev*. 2021;50(15):8762–8789. doi:10.1039/d1cs00074h
39. Wang Q, Zhu L, Xing F, Zhao P, Wang F. The comparison of the effects of local cooling and heating on apoptosis and pyroptosis of early-stage pressure ulcers in rats. *J Cell Biochem*. 2020;121(2):1649–1663. doi:10.1002/jcb.29399
40. Zhu K, Qian S, Guo H, et al. pH-activatable organic nanoparticles for efficient low-temperature photothermal therapy of ocular bacterial infection. *ACS Nano*. 2022;16(7):11136–11151. doi:10.1021/acsnano.2c03971
41. Bruxel MA, Tavares AMV, Zavarize Neto LD, et al. Chronic whole-body heat treatment relieves atherosclerotic lesions, cardiovascular and metabolic abnormalities, and enhances survival time restoring the anti-inflammatory and anti-senescent heat shock response in mice. *Biochimie*. 2019;156:33–46. doi:10.1016/j.biochi.2018.09.011
42. Pettinger J, Le Bihan YV, Widya M, van Montfort RL, Jones K, Cheeseman MD. An irreversible inhibitor of HSP72 that unexpectedly targets lysine-56. *Angew Chem Int Ed Engl*. 2017;56(13):3536–3540. doi:10.1002/anie.201611907
43. Pan Z, Wu Q, Xie Z, Wu Q, Tan X, Wang X. Upregulation of HSP72 attenuates tendon adhesion by regulating fibroblast proliferation and collagen production via blockade of the STAT3 signaling pathway. *Cell Signal*. 2020;71:109606. doi:10.1016/j.cellsig.2020.109606
44. Park G, Yoon BS, Moon JH, et al. Green tea polyphenol epigallocatechin-3-gallate suppresses collagen production and proliferation in keloid fibroblasts via inhibition of the STAT3-signaling pathway. *J Invest Dermatol*. 2008;128(10):2429–2441. doi:10.1038/jid.2008.103
45. Wang L, Astone M, Alam SK, et al. Suppressing STAT3 activity protects the endothelial barrier from VEGF-mediated vascular permeability. *Dis Model Mech*. 2021;14(11). doi:10.1242/dmm.049029
46. Marber MS, Latchman DS, Walker JM, Yellon DM. Cardiac stress protein elevation 24 hours after brief ischemia or heat stress is associated with resistance to myocardial infarction. *Circulation*. 1993;88(3):1264–1272. doi:10.1161/01.cir.88.3.1264
47. Luo X, Tao L, Lin P, Mo X, Chen H. Extracellular heat shock protein 72 protects Schwann cells from hydrogen peroxide-induced apoptosis. *J Neurosci Res*. 2012;90(6):1261–1269. doi:10.1002/jnr.22810
48. Zhang Y, Wiesholler LM, Rabie H, et al. Remote control of neural stem cell fate using NIR-responsive photoswitching upconversion nanoparticle constructs. *ACS Appl Mater Interfaces*. 2020;12(36):40031–40041. doi:10.1021/acsmi.0c10145
49. Li Y, Zhang Z, Xu K, et al. Minocycline alleviates peripheral nerve adhesion by promoting regulatory macrophage polarization via the TAK1 and its downstream pathway. *Life Sci*. 2021;276:119422. doi:10.1016/j.lfs.2021.119422
50. Lan SM, Yang CC, Lee CL, Lee JS, Jou IM. The effect of molecular weight and concentration of hyaluronan on the recovery of the rat sciatic nerve sustaining acute traumatic injury. *Biomed Mater*. 2017;12(4):045024. doi:10.1088/1748-605X/aa6f1a
51. Riccio M, Marchesini A, Pugliese P, De Francesco F. Nerve repair and regeneration: biological tubulization limits and future perspectives. *J Cell Physiol*. 2019;234(4):3362–3375. doi:10.1002/jcp.27299

International Journal of Nanomedicine

Dovepress

## Publish your work in this journal

The International Journal of Nanomedicine is an international, peer-reviewed journal focusing on the application of nanotechnology in diagnostics, therapeutics, and drug delivery systems throughout the biomedical field. This journal is indexed on PubMed Central, MedLine, CAS, SciSearch®, Current Contents®/Clinical Medicine, Journal Citation Reports/Science Edition, EMBASE, Scopus and the Elsevier Bibliographic databases. The manuscript management system is completely online and includes a very quick and fair peer-review system, which is all easy to use. Visit <http://www.dovepress.com/testimonials.php> to read real quotes from published authors.

Submit your manuscript here: <https://www.dovepress.com/international-journal-of-nanomedicine-journal>